2nd Symposium on New Trends in Nuclear and Medical Physics, Poland, September 24–26, 2025

Classification of Signal Events for Entanglement Studies with J-PET Using Machine Learning Techniques

D. Kumar[a,b,c,*], S. Sharma[a,b,c] and P. Moskal[a,b,c]

[a] *Faculty of Physics, Astronomy, and Applied Computer Science, Jagiellonian University, Łojasiewicza 11, 30-348 Kraków, Poland*
[b] *Total-Body Jagiellonian-PET Laboratory, Jagiellonian University, Łojasiewicza 11, 30-348, Kraków, Poland*
[c] *Center for Theranostics, Jagiellonian University, Kopernika 40, 31-501 Kraków, Poland*

Doi: 10.12693/APhysPolA.148.S105 *e-mail: d.kumar@doctoral.uj.edu.pl

Understanding the entangled polarization of photons produced in positron–electron annihilation remains experimentally challenging. Recently, it has been proposed to utilize this correlation in positron emission tomography imaging to suppress the random background and as a diagnostic parameter. Conventional positron emission tomographs rely on the registration of the two annihilation photons from positron annihilation. However, measuring polarization correlations requires scattering of annihilation photons in the detector volume and the registration of their corresponding scatters. Such a 4-hit event topology inherently suffers from low efficiency and high background. Therefore, translating this quantum information into medical imaging requires a method to overcome the inherent limitations of conventional geometric cuts. We present a machine learning classification framework trained on simulated detector events. This approach enables a high-purity separation of polarization-correlated signal from background and simultaneously achieves a significant improvement in computational efficiency.

topics: Jagiellonian positron emission tomography (J-PET), machine learning, entanglement

1. Introduction

The study of entangled photons in the high-energy regime is important for both fundamental physics and medical physics [1–3]. Recently, it has been a subject of intensive investigations [4–19]. Positronium atom, a bound state of an electron and a positron, offers a natural source for these photons [3]. According to quantum electrodynamics prediction, annihilation photons from the singlet state of positronium decay exhibit entangled polarization [10–20]. Such an entangled nature can be accessed by measuring the correlation between their polarization states. In our recent studies, we observed the nonmaximal entanglement between photons when positrons annihilate in a porous polymer medium [10]. This led to the hypothesis that the strength of correlation might be environment-sensitive due to different annihilation mechanisms. These findings pave the way for further investigations into how this polarization correlation varies across different physical and chemical surroundings, potentially introducing new contrast mechanisms for quantum-enhanced positron emission tomography (QE-PET) imaging.

While the annihilation of positrons forms the basis of positron emission tomography (PET), this quantum property remains unexploited in PET imaging. Conventional PET relies on the detection of two back-to-back (511 keV each) photons [21]. Although there have been many advancements in PET imaging, the technique remains fundamentally limited by the difficulty of resolving scattered and random photons. The quantum correlation, sensitive to the annihilation medium, not only acts as a novel diagnostic probe but also holds the potential to reduce these backgrounds [7].

To access this correlation, the polarization states of photons must be measured. The high energy (511 keV) of these annihilation photons prohibits the use of traditional polarizers. The solution lies in exploiting the Compton scattering phenomenon as a polarization analyzer, governed by the Klein–Nishina cross-section [22]. This requires the 511 keV photons to get Compton-scattered in the PET detection unit, with the scattered photons also subsequently detected. In the last decades, several studies have reported the feasibility of measuring and utilizing this correlation to suppress background in reconstructed PET images. Crucially, the plastic scintillator-based PET system, such as the

Jagiellonian-PET (J-PET), is ideally suited for this research. J-PET is a multi-photon scanner that has application in multidisciplinary studies [23–27] and medicine [28–29]. It utilizes long plastic scintillator strips, which provide both a large detection volume and good time resolution [30–31]. The low atomic number (Z) of the plastic scintillator maximizes the cross-section for Compton scattering relative to photo-absorption, while the detector's high spatial and angular resolution allows for the precise localization of multiple scatter points. This allows the detector itself to function as the measurement apparatus. The strength of polarization correlation can be defined by the entanglement witness parameter R, which quantifies this strength [4, 10, 12, 32].

The measurement of the entanglement witness, R, requires isolating the specific 4-hit event topology (one Compton scatter per annihilation photon) with high precision. This critical event selection process is currently challenged by background noise, complex random coincidences, and inherently low efficiency due to the strict kinematic requirements. With the advancement of new tools for data analysis and machine learning-based approaches, various algorithms can be used to improve accuracy in event classification. Machine learning (ML)-based classification has proven effective in various applications in high-energy physics. To address the severe purity–efficiency trade-off, this work introduces an ML approach [33]. By leveraging the deep pattern recognition capabilities of ML, we aim to isolate the required 4-hit physical signature with high purity. This will ensure the reliability of the R measurement, while simultaneously enhancing the computational efficiency essential for clinical translation.

2. Event topology

The dataset used in this study was generated using J-PET Geant4, a J-PET simulation package, based on the Geant4 toolkit. For a more realistic simulation, all possible decay channels of positron annihilation in porous medium were included. Simulated events were further analyzed using the J-PET framework to introduce source activity, smearing parameters, and coincidence time window. The analysis method is described in [10]. To measure entanglement between two photons (their polarization correlation), both annihilation photons must scatter inside the detector. For this study, we selected the events with 4-hits: the first hit from each annihilation photon is the scatter site, and the second hit represents where the corresponding photon gets scattered. The following two selection criteria were applied to identify and refine 4-hit events:

(i) Geometric coincidence. We selected events in a coincidence time window of 20 ns that registered at least four hits in the detector to maximize efficiency, thus avoiding the loss of true signal events that might be accompanied by background noise.

(ii) Energy-based pre-selection. From this pool, a candidate 4-hit event is constructed by identifying and selecting two hits defined as potential primary hits with energies between 200 and 340 keV and two hits defined as potential scatter hits with energies between 30 and 200 keV. These specific energy cuts are crucial for isolating valid scattering events and accurately simulating the experimental setup. The 30 keV lower bound is applied to emulate the detector's operational energy threshold used in the experiment. The 340 keV upper bound is chosen because it closely corresponds to the Compton edge for 511 keV photons.

3. Methodology

The current methods for finding events use simple, step-by-step selection criteria. Such a sequential approach often misses the hidden or complicated patterns of the signal, and the resultant efficiency is often very low. To fix the issue of high background and low efficiency, we developed and demonstrated here an event selection method — a binary classification system powered by the Python data science tools [34, 35]. The training and testing data were created using a detailed Geant4 Monte Carlo simulation of the J-PET 3-layer prototype geometry. This simulation gave us the ground truth, identifying exactly which 4-hit events were true signals and which were background.

The underlying physics of the four hits can be described by 20 independent parameters (position, time, and energy for each of the four hits). However, the subsequent analysis utilizes a set of 30 correlated features derived from these parameters. The events used for ML classification were the preselected candidates identified in the previous section. Each event was then described by a 30-feature vector (a list of 30 characteristics), which focuses on kinematic and timing information. The full 30-feature vector is composed of grouped metrics:

- Hit position features (12 features).
  The X, Y, and Z coordinates for all four hits (two primary and two scatter hits).
- Derived kinematic features (4 features).
  The X, Y, and Z coordinates of the reconstructed annihilation point, plus the angle between the primary photon directions.
- Time and distance features (14 features).
  The time and distance differences between the two primary hits, and the time and distance differences between each of the four possible primary-scatter hit pairs (time-of-flight information).

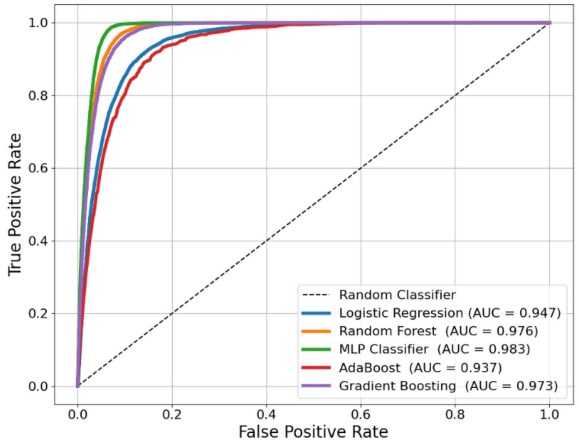

Fig. 1. ROC curve comparing the performance of the five machine learning models (logistic regression, random forest, multi-layer perceptron (MLP), AdaBoost, and gradient boosting) against a non-discriminating random classifier (area under the curve, AUC = 0.5). The curve illustrates the trade-off between the true positive rate and the false positive rate for various probability thresholds. The MLP classifier, with an AUC of 0.983, achieved the highest performance to separate the true 4-hit Compton signal from background noise.

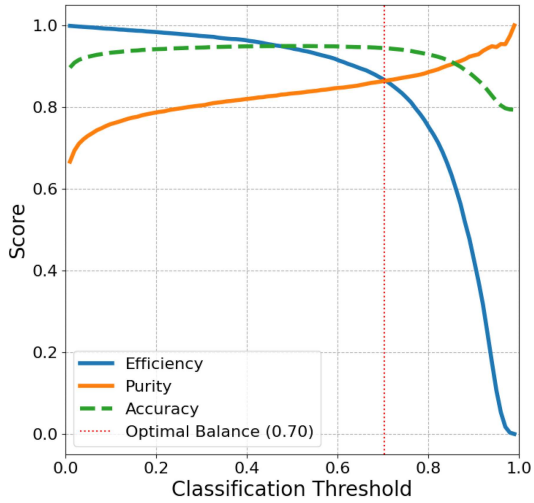

Fig. 2. Plot illustrating the key performance metrics, i.e., purity efficiency and accuracy, as a function of the classification probability threshold (T) for the optimized multi-layer perceptron (MLP) model. The optimal threshold used for the final classification was determined at T = 0.70, which represents the highest combined performance, prioritizing both high purity (86.39%) and high efficiency (86.69%) for the selected event sample. This demonstrates the model's ability to balance data quality and event retention.

This includes the precise spatial location of all four hits, time differences between pairs of hits (time-of-flight information), and distance between the hits, the angle between primary photon directions, and the position of the reconstructed annihilation point.

Before training, all features were standardized using a `StandardScaler()` function (from the scikit-learn library) [34, 35]. This scaling step is critical for the chosen deep neural network (DNN) classifier, as it normalizes the feature space, ensuring equal contribution from all inputs and accelerating the convergence of the gradient-based optimization process by preventing features with larger numerical ranges from dominating the updates.

The model's job was to identify true "4-hit Compton (signal) events", consistent with the desired dual scattering pattern and random coincidences (background), including accidental hits and complex scattering.

3.1. Model selection and hyperparameter tuning

We tested several models to find the most effective classifier for this complex selection task, including random forest (RF), eXtreme Gradient Boosting (XGBoost), and a deep neural network (DNN) [36–40]. The performance of these models, after extensive hyperparameter tuning, is compared using the receiver operating characteristic (ROC) curve analysis (see Fig. 1) [41].

The best results were consistently achieved by the multi-layer perceptron (MLP) classifier, a type of deep neural network (DNN). This model was ultimately selected because the relationships between the 30 input features are highly complex and non-linear, a domain where deep learning excels compared to traditional ensemble methods. The final MLP structure was optimized using the scikit-learn library in Python, achieving a best cross-validation accuracy of 94.90% [34]. The optimal hyperparameters selected for the final classifier included two hidden layers with 15 neurons each, an L2 regularization term ($\alpha = 0.0001$), and a maximum of 300 iterations, utilizing the default ReLU activation function and Adam solver. This tuning process led to an ideal probability threshold of T = 0.70, which yielded the optimal balance between data purity and efficiency (see Fig. 2).

3.2. Feature importance

While the MLP provides the highest accuracy, its internal structure is complex and difficult to interpret. To understand which of the 30 features were most valuable in separating signal from background, we used the random forest (RF) model [38]. The RF classifier, which uses the Gini impurity index as its splitting criterion, allows for the calculation of feature importance scores. The resulting analysis

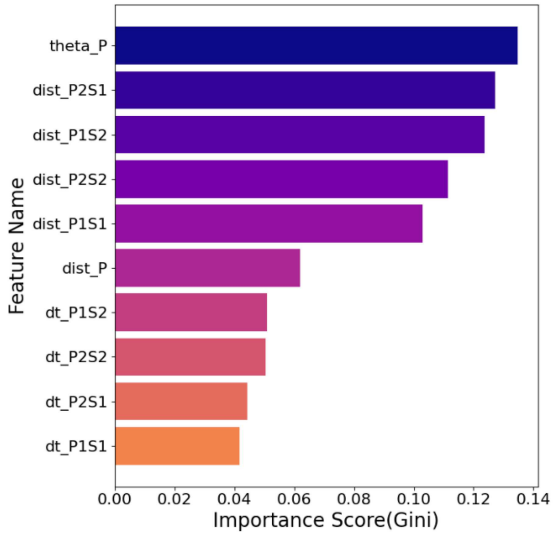

Fig. 3. Feature importance scores derived from the random forest (RF) classifier, ranked by the Gini impurity index. Only the top 10 most influential features are shown. Feature labels: theta_P — angle between direction of two primary hits; dist_PxSy — distance between a primary hit (P$_x$) and a scatter hit (S$_y$) (e.g., dist_P2S1 is the distance between the second primary candidate and the first scatter candidate); dist_P — distance between two primary hit candidates; dt_PxSy — time difference (Δt) between a primary hit (P$_x$) and a scatter hit (S$_y$).

identified the angle between the primary hits and the distance between the primary and scatter hits as the most crucial features for event discrimination (see Fig. 3).

3.3. Classification performance and efficiency

The performance of traditional, fixed-cut analysis serves as our crucial baseline. As illustrated in Fig. 1 by the ROC curve, the MLP classifier clearly demonstrates superior classification ability compared to other tuned models [40]. Using the same simulated dataset, the fixed-cut method, even after applying further kinematic criteria (e.g., angular cuts, annihilation point criteria for primary hits) to improve event association, yields an initial purity of 34.91% (meaning approximately 35% of all selected events are true signal) and an efficiency of 13.71% (meaning only 13.7% of all true signal events are retained).

In contrast, the final MLP model performed excellently, achieving an overall success rate of 94.94% on unseen data. Most importantly for the quantum correlation measurement, the purity of our selected signal events hit 86.39%. This represents a substantial improvement over the traditional methods, increasing event purity by approximately 50 percentage points compared to the baseline. The model's efficiency was also very high at 86.69%, representing a significant gain in event retention compared to the sequential cut-based 13.71% efficiency.

The subsequent critical step in the overall analysis chain is associating the scatter hits with their respective primary hits. Traditional methods for this association increase purity significantly (by more than a factor of two, depending upon the method used) but result in a large loss of signal, decreasing efficiency by over 50% [42]. While this association step is not included in the current ML-based work, the high purity and efficiency achieved by the MLP in this first stage provide a robust foundation, and we assume these advantages will be maintained even after the final association criteria are applied.

4. Conclusions

The practical application of the entangled nature of annihilation photons in PET imaging requires high event purity, an efficient event analyzer, and fast processing. We demonstrate that a deep neural network (DNN) classifier can effectively sort the complex 4-hit data from J-PET scanners, providing high-quality data for polarization correlation studies.

Future efforts will focus on expanding this machine learning methodology to the subsequent, equally challenging stage of event processing, i.e., the association of scatter hits to their correct primary photon paths, which is necessary for full event reconstruction. Following the successful validation on simulated data, this MLP-based selection method will be applied directly to experimental J-PET data and adapted for use with the modular J-PET detector setup.

Acknowledgments

We acknowledge support from the National Science Centre of Poland through grants MAESTRO no. 2021/42/A/ST2/00423, OPUS no. 2021/43/B/ST2/02150, SONATA no. 2023/50/E/ST2/00574, PRELUDIUM no. 2024/53/N/ST2/04279, the Ministry of Science and Higher Education through grant no. IAL/SP/596235/2023, European Union within the Horizon Europe Framework Programme (ERC Advanced Grant POSITRONIUM no. 101199807), the SciMat and qLife Priority Research Areas budget under the program Excellence Initiative — Research University at Jagiellonian University. We also acknowledge the Polish high-performance computing infrastructure PLGrid (HPC Center: ACK Cyfronet AGH) for providing computer facilities and support within the computational grant no. PLG/2024/017688.

References

[1] P. Moskal, *Physics* **17**, 138 (2024).

[2] P. Moskal, in: *Proc. 2018 IEEE Nuclear Science Symp. and Medical Imaging Conf. (NSS/MIC 2018)*, IEEE, 2018.

[3] S.D. Bass, S. Mariazzi, P. Moskal, E. Stępień, *Rev. Mod. Phys.* **95**, 021002 (2023).

[4] I. Tkachev, S. Musin, D. Abdurashitov, A. Baranov, F. Guber, A. Ivashkin, A. Strizhak, *Sci. Rep.* **15**, 6064 (2025).

[5] G.R. Romanchek, G. Shoop, M.A. Kupinski, P.H. Kuo, M. King, L.R. Furenlid, S. Abbaszadeh, *Bio-Algorithms Med-Syst.* **20**, 27 (2024).

[6] P. Caradonna, *Ann. Phys.* **470**, 169779 (2024).

[7] G. Romanchek, G. Shoop, S. Abbaszadeh, *Bio-Algorithms Med-Syst.* **19**, 9 (2023).

[8] S. Parashari, D. Bosnar, I. Friščić, A.M. Kožuljević, Z. Kuncic, P. Žugec, M. Makek, *Phys. Lett. B* **852**, 138628 (2024).

[9] D. Kim, A.N. Rachman, U. Taisei, M. Uenomachi, K. Shimazoe, H. Takahashi, *J. Instrum.* **18**, P07007 (2023).

[10] P. Moskal, D. Kumar, S. Sharma et al., *Sci. Adv* **11**, 3046 (2025).

[11] A. Ivashkin, D. Abdurashitov, A. Baranov, F. Guber, S. Morozov, S. Musin, A. Strizhak, I. Tkachev, *Sci. Rep.* **13**, 7559 (2023).

[12] D.P. Watts, J. Bordes, J.R. Brown, A. Cherlin, R. Newton, J. Allison, M. Bashkanov, N. Efthimiou, N.A. Zachariou, *Nat. Commun.* **12**, 2646 (2021).

[13] D. Abdurashitov, A. Baranov, D. Borisenko et al., *J. Instrum.* **17**, P03010 (2022).

[14] S. Sharma, D. Kumar, P. Moskal, *Acta Phys. Pol. A* **142**, 428 (2022).

[15] P. Caradonna, K. Shimazoe, *Phys. Rev. A* **112**, 032413 (2025).

[16] P. Caradonna, I. D'amico, D.G. Jenkins, D.P. Watts, *Phys. Rev. A* **109**, 033719 (2024).

[17] P. Knights, F. Ryburn, G. Tungate, K. Nikolopoulos, *Eur. J. Phys.* **39**, 025203 (2018).

[18] G. Romanchek, G. Shoop, K. Gholami, E. Enlow, S. Abbaszadeh, *IEEE Trans. Radiat. Plasma Med. Sci.* **8**, 916 (2024).

[19] A.M. Kožuljević, T. Bokulić, D. Grošev, S. Parashari, L. Pavelić, M. Rade, M. Marijaň, Z. Zuvić, M. Makek, arXiv:2510.11504 (2025).

[20] C.S. Wu, I. Shaknov, *Phys. Rev.* **77**, 136 (1950).

[21] A. Alavi, T. J. Werner, E. Stępień, P. Moskal, *Bio-Algorithms Med-Syst.* **17**, 203 (2021).

[22] O. Klein, T. Nishina, *Z. Phys.* **52**, 853 (1929).

[23] P. Moskal, A. Gajos, M. Mohammed et al., *Nat. Commun.* **12**, 5658 (2021).

[24] P. Moskal, K. Dulski, N. Chug et al., *Sci. Adv.* **7**, 4394 (2021).

[25] P. Moskal, E. Czerwiński, J. Raj et al., *Nat. Commun.* **15**, 78 (2024).

[26] P. Moskal, J. Baran, S. Bass et al., *Sci. Adv.* **10**, 2840 (2024).

[27] P. Moskal, D. Alfs, T. Bednarski et al., *Acta Phys. Pol. B* **47**, 509 (2016).

[28] P. Moskal, E. Stępień, A. Khreptak, *Bio-Algorithms Med-Syst.* **20**, 55 (2024).

[29] P. Moskal, E. Stępień, *PET Clin.* **15**, 439 (2020).

[30] S. Niedźwiecki, P. Białas, C. Curceanu et al., *Acta Phys. Pol. B* **48**, 1567 (2017).

[31] P. Moskal, O. Rundel, D. Alfs et al., *Phys. Med. Biol.* **61**, 2025 (2016).

[32] D. Kumar, S. Sharma, P. Moskal, *J. Phys. Conf. Ser.* **3029**, 012006 (2025).

[33] P. Baldi, P. Sadowski, D. Whiteson, *Nat. Commun.* **5**, 4308 (2014).

[34] F. Pedregosa, V. Michel, O. Grisel et al., *J. Mach. Learn. Res.* **12**, 2825 (2011).

[35] W. McKinney, in: *Proc. of the 9th Python in Science Conf.*, 2010.

[36] T. Chen, C. Guestrin, in: *Proc. of the ACM SIGKDD Int. Conf. on Knowledge Discovery and Data Mining*, 2016, p. 785.

[37] J.H. Friedman, *Ann. Statist.* **29**, 1189 (2001).

[38] L. Breiman, *Mach. Learn.* **45**, 5 (2001).

[39] D.W. Hosmer, S. Lemeshow, R.X. Sturdivant, *Applied Logistic Regression*, 3rd ed., John Wiley & Sons 2013.

[40] I. Goodfellow, Y. Bengio, A. Courville, J. Heaton, *Genet. Program. Evol. Mach.* **19**, 305 (2017).

[41] T. Fawcett, *Pattern Recognit. Lett.* **27**, 861 (2006).

[42] D. Kumar, S. Sharma, P. Moskal, *Proc. Sci.* **449**, 564 (2024).